Chemie der Erde xxx (2012) xxx–xxx

Contents lists available at SciVerse ScienceDirect

Chemie der Erde

journal homepage: www.elsevier.de/chemer

# Weathering of Sb-rich mining and smelting residues: Insight in solid speciation and soil bacteria toxicity

Alexandra Courtin-Nomade[a,*], Ony Rakotoarisoa[a], Hubert Bril[a], Malgorzata Grybos[a], Lionel Forestier[b], Frédéric Foucher[c], Martin Kunz[d]

[a] Université de Limoges, GRESE, E.A. 4330, IFR 145 GEIST, F.S.T., 123 Avenue A. Thomas, 87060 Limoges Cedex, France
[b] Université de Limoges, UGMA, UMR 1061, IFR 145 GEIST, F.S.T., 123 Avenue A. Thomas, 87060 Limoges Cedex, France
[c] Centre de Biophysique Moléculaire, CNRS-OSUC, Rue Charles Sadron, 45071 Orléans, France
[d] Advanced Light Source, Lawrence Berkeley National Lab, 1 Cyclotron Road, Berkeley, CA 94720, United States

ARTICLE INFO

*Article history:*
Received 14 December 2011
Accepted 19 February 2012

*Keywords:*
Mine tailings
Slags
Antimony
Arsenic
Solid speciation
Toxicity
Bacterial communities
Iron (hydr-)oxides
Tripuhyite
Jarosite

ABSTRACT

Tailings and slag residues from the most important antimony mine of the French Massif Central were analysed for their mineralogical and chemical contents by conventional X-ray powder diffraction and synchrotron-based X-ray microdiffraction (μ-XRD). Results show that ~2000 metric tons of Sb are still present at the abandoned mining site. Mean concentrations of Sb in slags and tailings are 1700 and 5000 mg kg$^{-1}$, respectively. In addition, smaller quantities of As were also measured (~800 mg kg$^{-1}$ in tailings). Toxicity tests of As and Sb indicate that the growth of bacteria is severely affected at these concentrations. In particular, Sb was observed to cause negative effects for several types of bacteria. Almost all primary minerals carrying trivalent Sb disappeared during weathering at the expense of phases in which $Sb^{5+}$ is the most abundant form. Instead of sulphides, Sb-bearing Fe hydroxides (goethite and lepidocrocite) are now present in the residues together with Sb-bearing jarosite and Sb(-Fe) oxides and hydroxides such as tripuhyite, senarmontite, romeite, cervantite, and valentinite. Water analyses of the main local stream indicate little remobilization of Sb downstream the site and despite the acidic pH of the surface tailings, pH values show neutral or near-neutral values on all locations of the site.


## 1. Introduction

Both historical metallurgical areas and waste material related to mining exploitation and ore treatment contain significant amounts of heavy metals and metalloids. These sites represent one of the most important potential hazards for waters, biodiversity, and food chain. In recent years, several serious accidents have occurred in Europe, such as the failure of the main tailings dam in Aznalcollar (1998, Spain) (Grimalt et al., 1999; Hudson-Edwards et al., 2003), and, only two years later, the contamination of the Danube river at Bahia Mare in Romania (Macklin et al., 2003). Although these accidents prompted important changes to the European Seveso Directive (Directive 2003/105/EC of the European Parliament and of the Council of 16 December 2003 amending Council Directive 96/82/EC), new accidents are still happening, such as the toxic red sludge which escaped from a bauxite treatment unit near Ajka and flooded several Hungarian counties in 2010.

Beside these highly publicized disasters caused by physical dam failures which had physical (e.g., floods) and chemical (pollutions) consequences, other less well known chemical risks do exist. They are due to metal release from mechanically unstable and non-remediated mine tailings and from abandoned former mine galleries where wastes are submitted to atmospheric conditions, runoffs (underground, meteoric) or biotic effect (organisms living on the site or nearby). These alteration processes lead slowly but surely to contamination of the environment in addition to a continuous background level of contamination. They concern all of the metals and metalloids, particularly those which are considered toxic (such as As, Ni, Pb) or potentially toxic when they are highly concentrated in the mining areas and their surroundings. This accumulation may be attributed to the dispersion of particles (waste spreading), dissolution (physical erosion by rivers or winds) and/or atmospheric (smoke emissions) dispersion.

Antimony-dominant residues are reported near former mines (Flynn et al., 2003). The impact of the primary sulphide weathering can be attenuated by natural processes (e.g., dilution effects, iron or manganese oxides precipitation; Filella et al., 2009). Some previous studies have been performed to compare the fate of two metalloids, As and Sb, in highly concentrated mining sites from New South Wales (Australia; Ashley et al., 2003) and from the Southern French Massif Central (Casiot et al., 2007). Furthermore, the toxicity of Sb is often assumed to be similar to As, with $Sb^{3+}$ being more toxic

* Corresponding author. Tel.: +33 0 555 457 292; fax: +33 0 555 457 203.
*E-mail address:* alexandra.courtin@unilim.fr (A. Courtin-Nomade).

0009-2819/$ – see front matter © 2012 Published by Elsevier GmbH.
doi:10.1016/j.chemer.2012.02.004

than $Sb^{5+}$ (WHO, 2008). However, many key aspects of the environmental chemistry of Sb remain poorly understood as recently pointed out by Filella et al. (2009). Most of the previous Sb speciation studies concerned ores and mineralized veins (Wilson et al., 2004) and seemed to indicate a relationship between the concentration of $Sb^{5+}$ and the existence of $Fe^{3+}$ hydroxides (Ackermann et al., 2009; Scheinost et al., 2006; Takaoka et al., 2005; Wilson et al., 2004). Besides studies on soils affected by Sb (Mitsunobu et al., 2011; Murata et al., 2005), only little work has been done on the mineralogy of solid mining residues (Ashley et al., 2003, 2004; Craw et al., 2004; Majzlan et al., 2011; Wilson et al., 2004).

The aim of our present study is to (1) estimate the effects of dissolved As and Sb species on the growth of selected bacteria from non-contaminated soils (first step to assess the toxicity of these metalloids), (2) explain the presence of significant Sb concentrations in the dissolved fraction by studying mineralogical transformation processes affecting the solid residues, (3) compare the evolution of Sb-bearing phases from both flotation and smelting residues in order to further estimate the remediation scenarios and their sustainability in terms of modifications of *in situ* geochemical parameters, (4) compare the behaviour and fate of As and Sb and determine if iron oxides can lead to natural attenuation for Sb, as observed for As.

## 2. Geological context and ore deposits

The French Massif Central is the result of Variscan orogeny that occurred since the early Devonian in the studied area (Ledru et al., 1989; Bouchot et al., 2005). The Massif Central is mainly composed of metamorphic rocks such as migmatites, ortho- and paragneisses, which are all associated with amphibolites and locally intruded by small granitic bodies. Late Variscan faulting events favoured the emplacement of numerous hydrothermal ore deposits (gold and uranium mineralizations). The polymetallic district of "Brioude-Massiac" is composed of numerous veins scattered throughout Variscan metamorphic belts of the "Haut – Allier" series. Within the main metallogenic zones in this area, this district is known for its abundant mesothermal antimony ores (Bril et al., 1994) and is regarded as the best of its kind in France. The antimony ores were mainly exploited during the first part of the 20th century with around 39,000 metric tons of Sb metal extracted. The site of Ouche was the most productive among them (Périchaud, 1970), with more than 9000 metric tons mined and treated by flotation and metallurgical methods.

Ore is found in 2–3 m large sulphide-rich veins and lenses hosted in a quartz gangue with very low carbonate content and surrounded by biotite-rich paragneisses. The ores consist of rare arsenopyrite (FeAsS) and pyrite ($FeS_2$), abundant massive and well-crystallized stibnite ($Sb_2S_3$) with berthierite ($FeSb_2S_4$), rare native antimony and local sphalerite (ZnS) or more rarely Pb sulfosalts. Cementation processes affecting the ore bodies induced the formation of alteration products (secondary minerals) in the close vicinity of Sb-bearing sulphides such as red kermesite ($Sb_2S_2O$), beige to grey valentinite ($Sb_2O_3$) and yellow to orange ochres of antimony (Périchaud, 1970). With less than 2% of the whole paragenesis, these secondary minerals represent very small quantities.

Due to the lack of environmental legislation during the exploitation period, wastes were discarded throughout the entire district and abandoned on sites, submitted to climatic alteration with no remediation action undertaken until the end of 2011 for the Ouche site. Since September 2011, tailings have been covered with a geotextile liner and the access to the dump is closed by fences all around. Slags, however, are still observed near the site at the former smelter location and are fully accessible.

## 3. Materials and methods

### 3.1. Materials

The Ouche site is located near the small town of Massiac, 80 km south from Clermont-Ferrand, at an altitude of 500–700 m. In this region, climate is temperate (mean annual temperature ~8.6 °C; http://climat.meteofrance.com) with relatively variable temperatures, including cold winters and sparse rainfall (675 mm/year over the last 10 years; http://climat.meteofrance.com) uniformly distributed over the seasons.

Approximately ten ore veins were exploited near the village of Ouche. The tailings were disposed of in the deep and narrow "de Bussac" valley. This small valley is characterized by very steep slopes crosscut by former galleries where small water outlets are still visible. Samples of water were collected twice at seven locations (Fig. 2) in November 2010 (high flow period) and September 2011 (low flow period) at the end of the remediation works.

When solid samples were collected in 2009, the mine tailings formed a trapezoidal shaped heap with a flat top. Only very scarce vegetation developed on its surface and on the slopes (Fig. 1). The waste pile is 200 m long, 25 m large and 20 m high, representing an estimated volume of 200,000 metric tons of waste. Mill tailings consist in general of fine-grained material. They show some heterogeneities with coloured stratification in the millimetre to centimetre scale from light grey to bright orange or brown (Fig. 1). This is probably due to changes in ore composition and/or treatment processes when the heap was emplaced. Tailing samples were collected throughout the heap, mainly on or near the surface.

On the contrary to mill tailings, smelting residues are rare and observed as scattered slags or forming very small piles near the smelting site, ~200 m in front of the heap (near # 3, Fig. 2). Slag samples were chosen based on textural criteria, colour, and presence of alteration crusts or efflorescences on their surfaces.

### 3.2. Analytical techniques for dissolved and solid fraction

Samples of the dissolved fraction were filtered with 0.45 μm acetate cellulose filters, then acidified with $HNO_3$ prior to analyses by ICP-MS/OES (ACME, certified laboratory, Canada) for samples collected in November 2010 or by AAS for samples from September 2011 (GRESE laboratory, FR). Parameters such as temperature, pH, electrical conductivity (E.C.), and dissolved oxygen were measured on site.

Solid samples were analysed for mineralogical identification, textures, and chemical compositions using optical microscopy, scanning electron microscopy (SEM), and electron probe microanalysis (EPMA) on polished 30 μm thick thin-sections. Mill tailings were embedded using an epoxy resin (see Courtin-Nomade et al., 2010 as an example of the protocol). Dried tailing samples were mixed with deionised water at a ratio of 2 g soil to 5 ml, and shaken vigorously for 30 min and finally left still for 30 min. The pH values of these mixtures were then measured using a Metrohm 632 pH meter with a KCl filled microelectrode.

Secondary electron (SE) and back-scattered electron (BSE) images were obtained with a Philips XL-30 scanning electron microscope (SEM) equipped with an energy dispersive X-ray analyzer (EDAX) for morphological and semi-quantitative chemical information (SERMIEL, Limoges, FR). Electron probe microanalysis was performed with a CAMECA SX-50 equipped with an EDAX system and 4 wavelength-dispersive spectrometers operating at 15 kV and 6 nA beam current at the ISTO facility (Orléans, FR) giving a volume of analysis of about 1 $\mu m^3$. The microprobe was calibrated using standard reference materials including natural and synthetic silicates, oxides, and sulfide minerals. Counting time for the various elements ranges from 10 to 40 s according to their abundance. Bulk and micro-X-ray diffraction were performed to assess the mineralogy of the materials. A RIGAKU JEI JERT apparatus using a CuKα radiation (step size = 0.02°2$\theta$; counting time = 5 s/step, between 4° and 80°2$\theta$) and equipped with a diffracted-beam graphite monochromator to minimize the fluorescence effect, was used for bulk powder X-ray diffraction at the ISTO facility (Tours, FR).

Synchrotron-based X-ray microdiffraction (μ-XRD) analyses were obtained on beamline 12.3.2, at the Advanced Light Source, Lawrence Berkeley National Lab (Berkeley, USA) (Kunz et al., 2009). Micro-XRD diffraction patterns were collected in reflection geometry on 30 μm thick thin-section mounted onto an XYZ translation stage horizontally tilted at 6°. Due to the small crystallite size, monochromatic mode was employed using an incident X-ray energy of 10 keV and a beam size of 2 μm (H) × 20 μm (V) (beam footprint size on the sample of 20 μm (H) × 20 μm (V) FWHM). A DECTRIS Pilatus 1 M pixel array detector served as diffraction detector. Geometric parameters were calibrated using corundum powder with the software XMAS (Tamura et al., 2005).

Micro-Raman spectroscopy (μRS) was performed using a Jobin Yvon 6400 Raman spectrometer (SPCTS, Limoges, FR), combined with a 100x objective which results in a spatial resolution of one micron. More experimental details on this setup have already been described in Courtin-Nomade et al., 2010. Further μRS analyses have been performed using a WITec 500RA atomic force microscope coupled with a confocal Raman spectrometer and a green laser (535 nm wavelength). This arrangement gives a spectral resolution of 3 $cm^{-1}$ and a spot size of 350 nm (CBM-CNRS, Orléans, FR).

Please cite this article in press as: Courtin-Nomade, A., et al., Weathering of Sb-rich mining and smelting residues: Insight in solid speciation and soil bacteria toxicity. Chemie Erde - Geochemistry (2012), doi:10.1016/j.chemer.2012.02.004

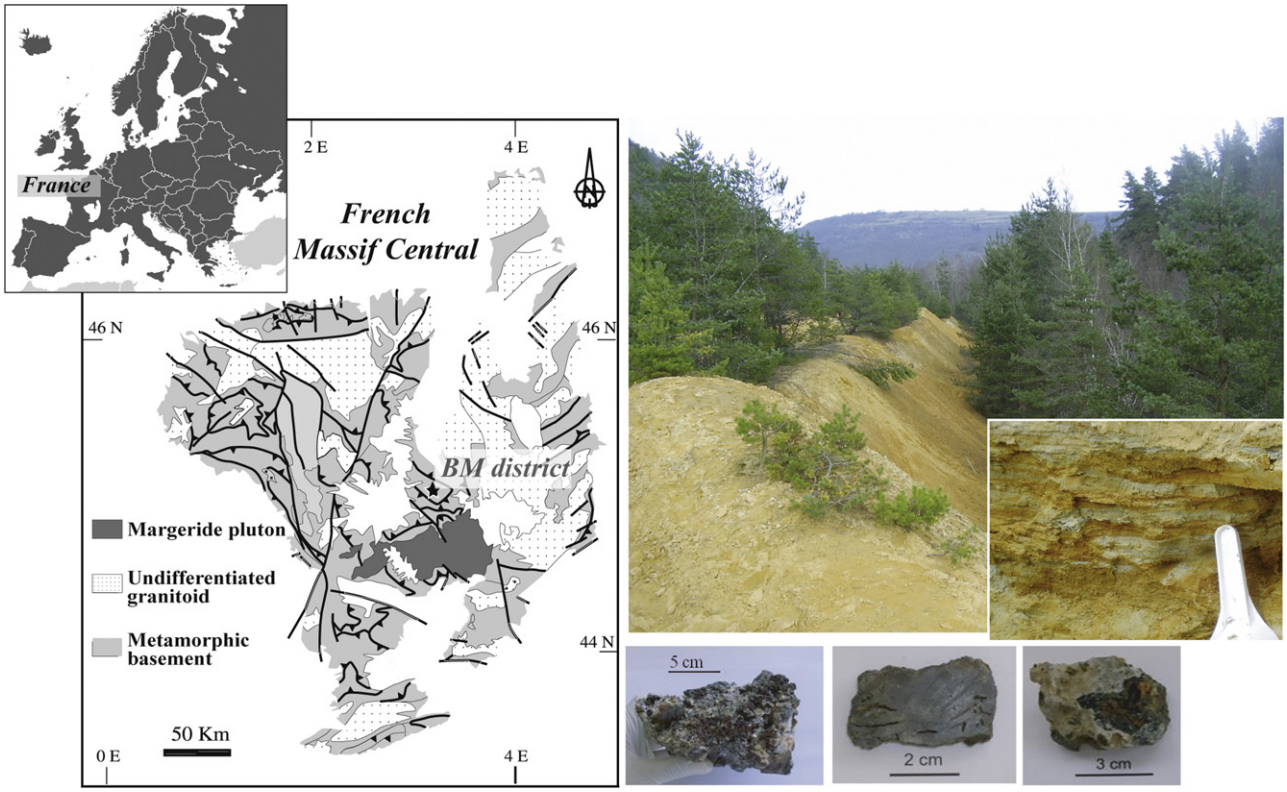


**Fig. 1.** Location of the French Massif Central and the Brioude-Massiac (BM) district. Photographs of the mine waste dump showing the stratification within the mill tailings and some of the collected slags near the former smelter.

### 3.3. Bacterial strains, culture media and incubation conditions

Bacteria were extracted from non-contaminated soils (6 strains, referred as NCS) and then tested for Sb and As toxicity. These prokaryotic microorganisms can be used as a model for predictions of the toxicity of chemicals/pollutants to the entire ecosystems (Wang et al., 2011). We focused on aerobic, heterotrophic bacteria because of their important role in soil processes and function (e.g., degradation of organic matter, weathering of minerals, excretion of plant nutrients). Isolated microbes were purified and phylogenetically analyzed by 16S rRNA amplification and sequencing. For this purpose, single bacterial colonies from agar plate were diluted in water and directly amplified in a 35-cycle PCR (Primus thermocycle, MWG) using the universal primers 16S-SP1 (5′ ACCTCCTTTCTAAGGAGCACC 3′) and 16-SP2 (5′ GATGCTCGCAACCACTATCCA 3′) as described in Therese et al. (2009). After ExoSapI (USB, Staufen, Germany) treatment, the PCR fragments were sequenced with 16S-SP1 and 16S-SP2 primers. Sequence reaction products were first analysed by the ABI 3130 and then by an automated DNA sequencer (Applied Biosystems, Carslbad, CA, USA). The nucleotide sequences were compared to sequences in the GenBank database using the BLAST algorithm. The closest known relatives (% sequence identity) are presented in Table 1.

### 3.4. Toxicity assay

All experiments were carried out in 24-well microplates filled with Luria-Bertani (LB) medium supplemented with various amounts of $Sb^{3+}$ and $As^{3+}$. Prior to the toxicity assays, bacteria were growing aerobically in LB broth at 28 °C with shaking to increase cellular biomass. After 48 h of incubation, the cells were washed 3-times in Milli-Q water, diluted again in LB medium to an optical density of 1 ($OD_{600}$ = 1) and 0.1 ml of each bacterial suspension was distributed into 2 ml-wells. Three wells were not inoculated to check the sterility of LB medium during the incubation period. Inoculated microplates were incubated for an additional 48 h. Growth of bacterial strains was estimated by monitoring the absorbance of suspensions at 600 nm using a UV visible spectrophotometer.

All suspensions, water and LB media used were sterilized by autoclaving (30 min at 121 °C). Solutions of $As^{3+}$ and $Sb^{3+}$ were prepared from sodium arsenite and potassium antimonyl tartrate, respectively. The final concentrations of Sb or As in microplate wells were: 0, 10, 50, 100, 200 and 1000 mg $l^{-1}$. The experiments were carried out in triplicate under aerobic conditions at 28 °C with stirring.

**Table 1**
Characteristics of bacterial strains isolated from non-contaminated soil (NCS) used in the toxicity assays.

| Bacterial strain | Closest match according | % Similarity | Gram |
|---|---|---|---|
| NCS1 | *Pseudomonas fluorescens* | 99 | G− |
| NCS2 | *Chryseobacterium taiwanense* | 96 | G− |
| NCS3 | *Pseudomonas poae* | 100 | G− |
| NCS4 | *Pseudomonas lurida* | 99 | G− |
| NCS5 | *Bacillus weihenstephanensis* | 99 | G+ |
| NCS6 | *Lysinibacillus sp.* | 98 | G+ |

## 4. Results

### 4.1. Microbiology

As shown in Table 1, four of six bacterial species were Gram-negative. All isolates were examined for their sensitivity to arsenite and antimonite using growth inhibition assay in liquid medium (LB medium and LB medium supplemented with various amount of dissolved $As^{3+}$ and $Sb^{3+}$). Since the growth of bacteria in LB broth was not perturbed by the presence of the elements, measured optical density at the end of incubation in LB broth ($OD_{LB}$) was compared to the optical density obtained at the end of incubation in LB broth enriched with $As^{3+}$ or $Sb^{3+}$ ($OD_{LBAs}$ or $OD_{LBSb}$). The impact factor for each bacterial strain was then calculated. The data are reported in Fig. 3. Three different effects could be assumed (i) those for which impact factor IF = 1: the presence of $As^{3+}$ or $Sb^{3+}$ has no effect on bacterial growth, (ii) those with IF > 1: the presence of $As^{3+}$ or $Sb^{3+}$ has stimulating effect on cells production and (iii) those with IF < 1: the presence of $As^{3+}$ or $Sb^{3+}$ has an inhibiting ("toxic") effect on biomass proliferation. As shown in Fig. 3, arsenite and antimonite have in general a negative effect on bacterial growth. The impact factors are <1 for a majority of tested bacteria even at relatively low metalloid concentrations. As an example, 10 mg $l^{-1}$ of $Sb^{3+}$ was sufficient to completely inhibit the growth of NCS2

Please cite this article in press as: Courtin-Nomade, A., et al., Weathering of Sb-rich mining and smelting residues: Insight in solid speciation and soil bacteria toxicity. Chemie Erde - Geochemistry (2012), doi:10.1016/j.chemer.2012.02.004

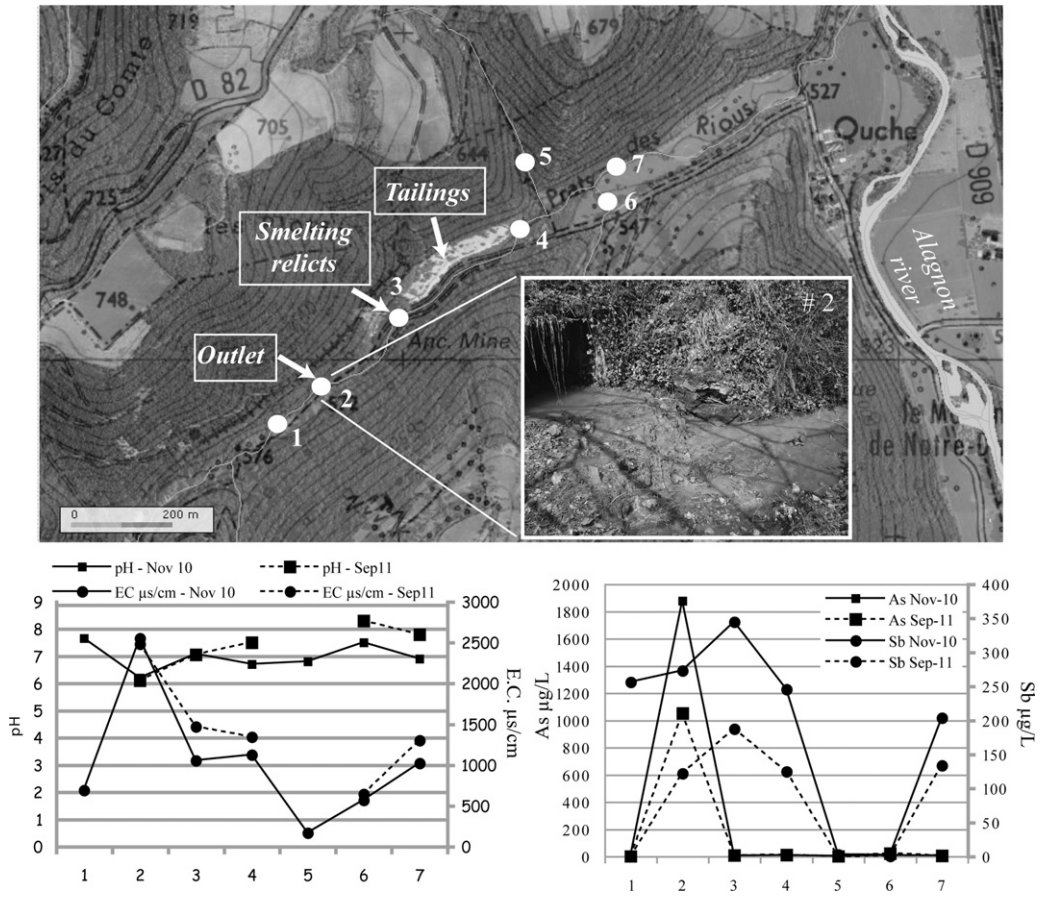


**Fig. 2.** Map of the former Ouche mine and locations of the sampling sites for the dissolved fractions; (b) pH and electrical conductivity (E.C.) evolution at the seven locations and variations of the As and Sb concentrations in the dissolved fraction in September 2010 (plain line) and November 2010 (dashed line).

(*Chryseobacterium taiwanense*); 50 mg $l^{-1}$ of $Sb^{3+}$ stopped the growth of NCS5 (*Bacillus weihenstephanensis*); 50 mg $l^{-1}$ of $As^{3+}$ decreased the growth of NCS3 (*Pseudomonas poae*) by 50%. However, for some isolates, the presence of $As^{3+}$ or $Sb^{3+}$ had a stimulating effect on cell proliferation. In the presence of antimonite, an impact factor >1 was observed for NCS3 (*Pseudomonas poae*) at 10 mg $l^{-1}$. In the presence of arsenite, a stimulating effect was observed for NCS1 (*Pseudomonas fluorescens*) at 50 mg $l^{-1}$.

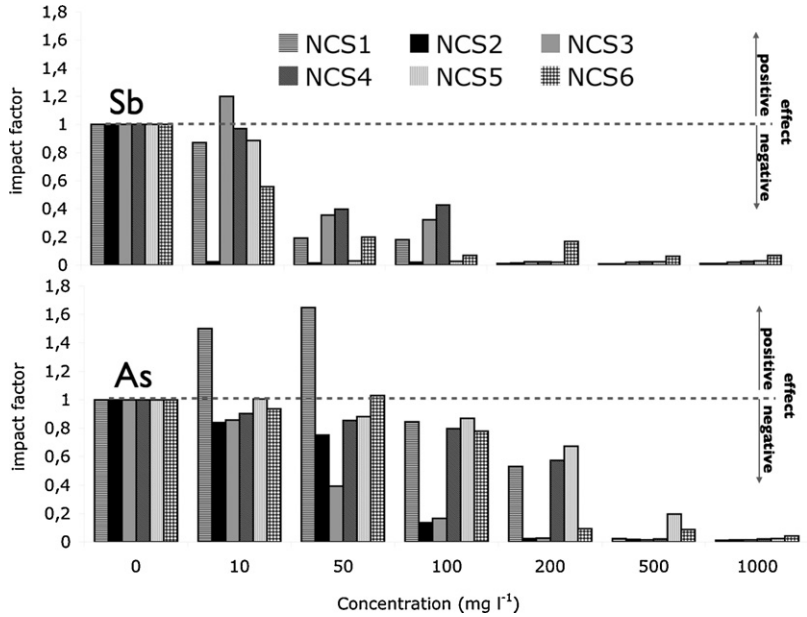


**Fig. 3.** Comparison of growth of 6 bacterial strains in the presence of various amounts of dissolved $Sb^{3+}$ and $As^{3+}$ performed in triplicates. Impact factor calculated optical density obtained at the end of incubation ($OD_{LBAs\ or\ Sb}$) divided by the optical density obtained at the same time in LB solely.

Please cite this article in press as: Courtin-Nomade, A., et al., Weathering of Sb-rich mining and smelting residues: Insight in solid speciation and soil bacteria toxicity. Chemie Erde - Geochemistry (2012), doi:10.1016/j.chemer.2012.02.004

### 4.2. Water parameters and chemistry, discharge of the de Bussac stream

The waste dump area is crossed by a small local river, receiving several other water inputs such as the mine water discharge (at the outlet #2) and small tributaries, non-affected by the mining activities, at locations #5 and 6 (Fig. 2).

The average measured pH values are ~7 (Fig. 2), including the outlet where the pH was the lowest at 6.2. On the contrary, the electrical conductivity (E.C.) is the highest at the outlet (2550 $\mu s\,cm^{-1}$; Fig. 2) and the lowest E.C. was measured for the reference small creek at #5 (168 $\mu s\,cm^{-1}$; Fig. 2). Antimony concentrations in waters are always high ($Sb_{mean} = 244.5 \pm 29.6\ \mu g\,l^{-1}$) except for locations #5 and 6 (2.7 and 2.4 $\mu g\,l^{-1}$, respectively) (Fig. 2). These small creeks do not cross mineralized veins, implying that the areas nearby were not impacted by mining activities. While the highest concentrations of As and Fe were measured at the outlet (1877 and 60,942 $\mu g\,l^{-1}$, respectively), Sb concentrations are maximal at #3 (near the former smelter; Sb = 344 $\mu g\,l^{-1}$). Similar trends for metal- or metalloid release have been observed for samples taken in November 2010 and September 2011. Measured values for pH and E.C. are very similar for these two periods.

### 4.3. Tailings and slags bulk chemical composition

The main fraction size of the tailings is between 200 and 50 μm (42%) while 92% of the tailings has a grain fraction within the 2000–20 μm range. Tailing and slag samples were all rich in silica, iron, and aluminium (Table 2). Metal and metalloid concentrations of the tailing samples are high for As (up to 1641.7 $mg\,kg^{-1}$), Ba (up to 2474 $mg\,kg^{-1}$), Pb (up to 774.8 $mg\,kg^{-1}$) and Sb (up to 11,560 $mg\,kg^{-1}$). Measured pH values of the tailings are acidic, around 2.6. In the slag samples, antimony is the main element among the metal(oids) (up to 5660 $mg\,kg^{-1}$). Total S concentrations, up to 1.32%, are twice as high as the highest concentration in tailing samples (Table 2).

### 4.4. Tailings mineralogy

The mineralogy of the tailings is dominated by gangue minerals such as quartz, albite, muscovite, clay minerals, and barite. Despite the dominance of the sulphides at the beginning of the tailings deposit, they are rarely reported nowadays with neither berthierite nor stibnite observed. The sulphide identified is always pyrite. Oxidation of the sulphides results in numerous secondary products containing Sb in different concentrations. They can be classified into three main types: sulphates, Fe (hydr-)oxides and (Fe-)Sb (hydr-)oxides. Some silicates may also contain minor Sb concentrations.

Sulphates have been identified by μRS and μXRD as jarosite, nominally $KFe_3(SO_4)_2(OH)_6$ (Figs. 4 and 5d). Jarosite is observed to form aggregates ranging from 10 to 50 μm in size, which in turn are composed of small grains or lamellar particles (Fig. 6a). This phase contains 5.9 ± 2.1% Sb and 0.7 ± 0.5% As on average (Table 3; Figs. 7 and 8). Smooth rings on the XRD patterns indicate that jarosite is cryptocrystalline and no change in its crystallinity is noted with varying Sb concentrations (Fig. 5d).

(Fe-)Sb (hydr-)oxides – The identification of FeSb (hydr-)oxides or Sb (hydr-)oxides was only possible by means of μ-XRD because of the high luminescence effect observed in μRS. FeSb (hydr-)oxides are mainly tripuhyite ($Fe^{3+}Sb^{5+}O_4$), which shows a very variable composition with Sb = 23 ± 5.9%, Fe = 26.1 ± 4.2% and minor concentration of As = 2.8 ± 1% (Table 3 and Fig. 7). Tripuhyite was identified as a poorly to well-crystalline phase (Fig. 5a & c). This mineral has a typical morphology, massive but with dehydration features (cracks). It often includes grains of other minerals such as quartz or goethite (Fig. 6a). In these phases, As seems to be strongly correlated to the Fe concentration with the highest As concentrations being measured for the highest Fe content. On the contrary to the very common tripuhyite, pure Sb oxides are very rare and have been identified as cervantite ($Sb^{3+}Sb^{5+}O_4$) usually associated with tripuhyite (Figs. 5c and 6a).

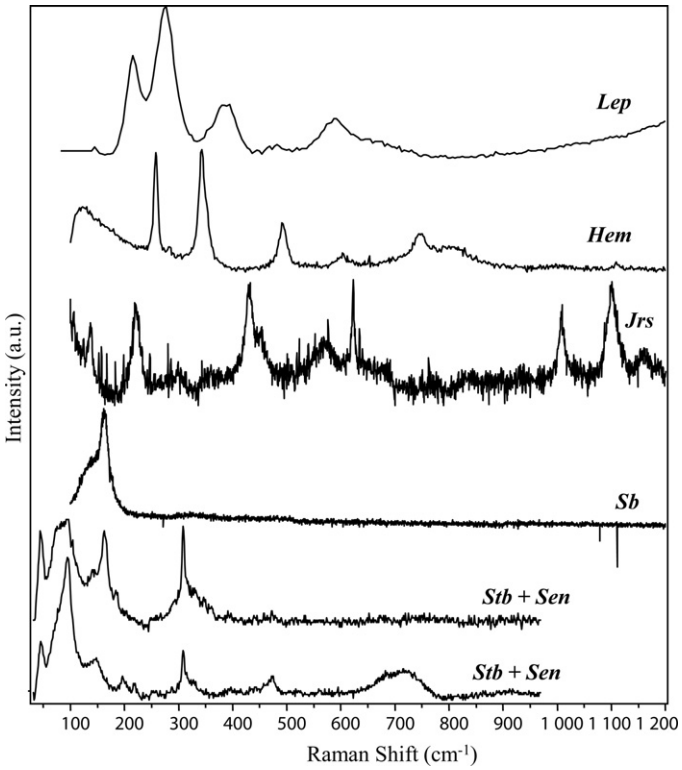


**Fig. 4.** Micro-Raman spectra of Sb-rich host phases. In the tailings they are identified as iron (oxy-)hydroxides (Hem: hematite; Lep: Lepidocrocite), Sb-bearing jarosite (Jrs). In the slags, we found native antimony (Sb) and stibnite (Stb) associated with senarmontite (Sen)).

Fe (hydr-)oxides – Antimony is also frequently associated to other secondary products resulting from weathering processes. Among them, iron (hydr-)oxides are widespread in the samples and the main species are well-crystalline goethite, hematite, and lepidocrocite. All of these Fe compounds (Fe = 39.9 ± 6.9%) contain Sb (6.8 ± 3.8%, up to 3% in hematite, between 3 and 14% in goethite and lepidocrocite) but not always As (Table 3 and Fig. 7).

### 4.5. Slag petrography and mineralogy

Slags are not abundant on the site. Indeed, they were used for the backfill of small roads in the surroundings because of their useful physical properties (among them, hardness and resistance to crushing). The remaining slag fragments are generally small in size with a well-developed porosity. Only a few samples show a glassy texture. They all exhibit weathering features, developed on their surface as efflorescences or as thin crusts covering the entire slag (Fig. 1). Slags are composed of minerals such as quartz and its high-temperature polymorphs (mainly cristobalite, but tridymite is also observed), feldspars (albite), sulphides (troilite, pyrite, stibnite), Ti oxides, and (Fe-)Sb oxides. Antimony-bearing phases were identified as well-crystalline romeite ($Ca_2Sb_2O_6OH$), senarmontite ($Sb_2O_3$), valentinite ($Sb_2O_3$), cervantite or clinocervantite, tripuhyite, and Fe (hydr-)oxides mainly in the form of hematite and goethite (Figs. 4 and 5e & f). Stibnite and senarmontite have been identified by μRS and μXRD. Senarmontite can be observed as inclusions in stibnite (Fig. 6b) or as individual grains.

Please cite this article in press as: Courtin-Nomade, A., et al., Weathering of Sb-rich mining and smelting residues: Insight in solid speciation and soil bacteria toxicity. Chemie Erde - Geochemistry (2012), doi:10.1016/j.chemer.2012.02.004

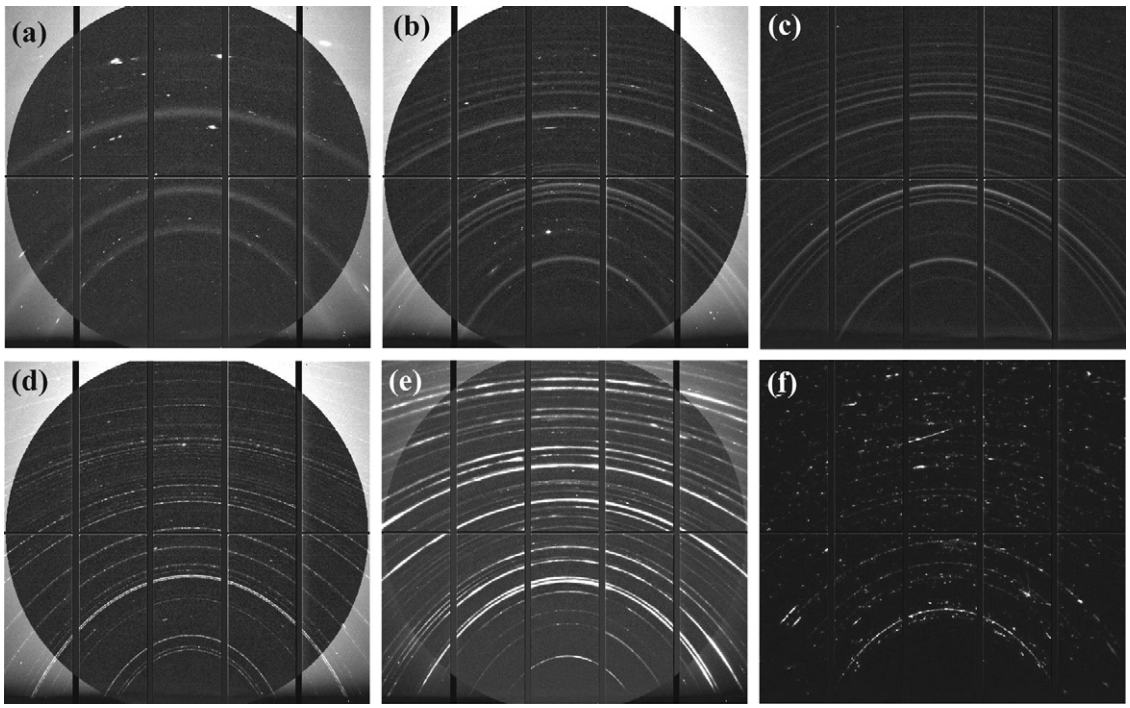


**Fig. 5.** Micro-X ray diffraction patterns of various Sb-bearing phases found in the tailings and slags. Tailings: (a) poorly crystalline tripuhyite, (b) Sb-rich goethite, (c) cervantite and well-crystalline tripuhyite, (d) jarosite. Slags: (e) senarmontite and valentinite; (f) cristobalite, tridymite and valentinite.

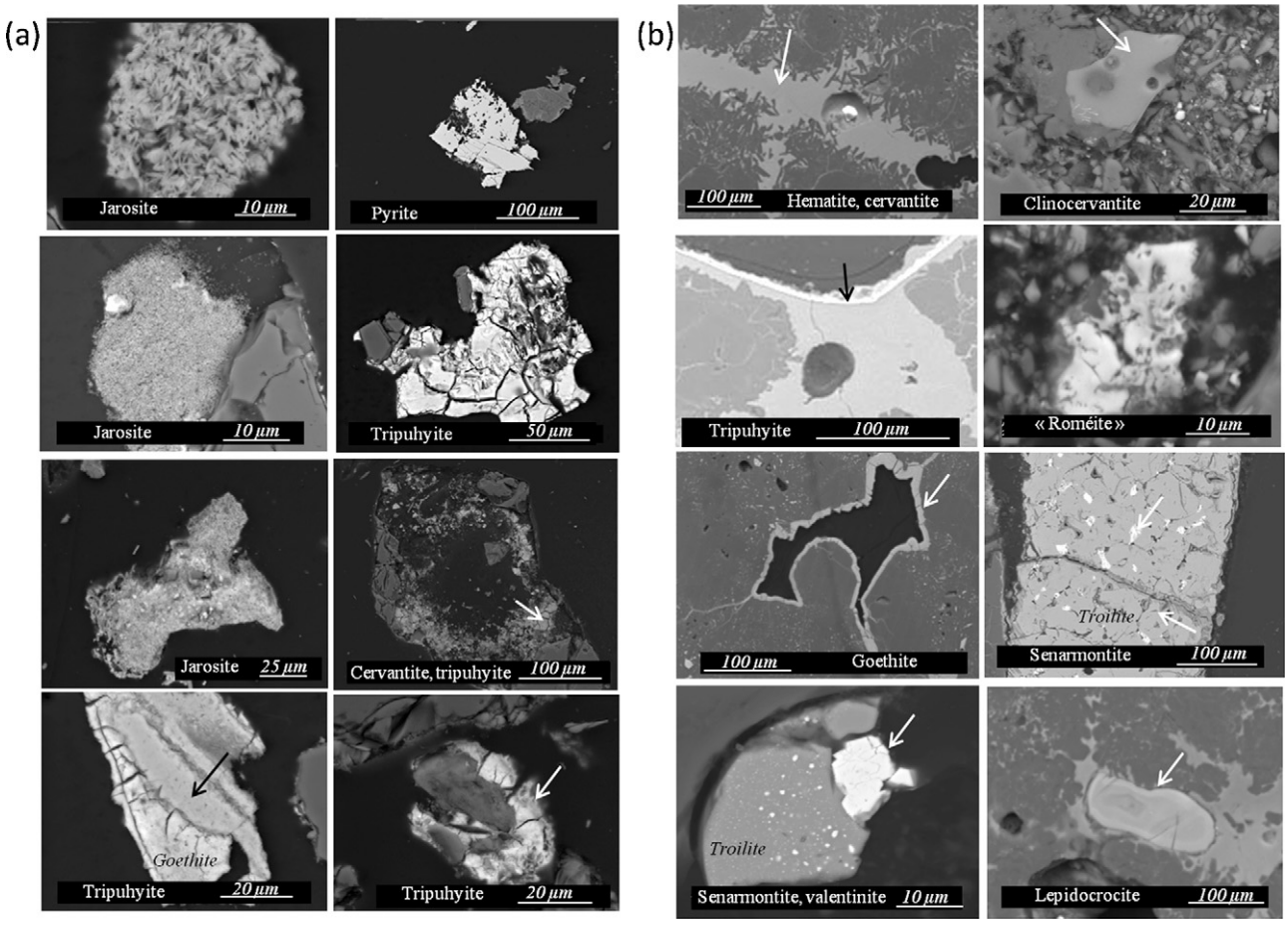


**Fig. 6.** Various morphologies of the Sb-host phases obtained by SEM (BSE) in (a) tailings and in (b) slags. The arrow indicates the phase mentioned in the black box.

Please cite this article in press as: Courtin-Nomade, A., et al., Weathering of Sb-rich mining and smelting residues: Insight in solid speciation and soil bacteria toxicity. Chemie Erde - Geochemistry (2012), doi:10.1016/j.chemer.2012.02.004

**Table 2**
Bulk composition (mean, maximum and minimum values in % or mg kg$^{-1}$) measured by ICP-MS/OES for slags and tailings.

| Element | Unit | MDL | Mean | | Max | | Min | |
|---|---|---|---|---|---|---|---|---|
| | | | Slags | Tailings | Slags | Tailings | Slags | Tailings |
| $SiO_2$ | % | 0.01 | 76.87 | 78.16 | 82.85 | 89.40 | 62.11 | 58.60 |
| $Al_2O_3$ | % | 0.01 | 7.52 | 8.55 | 10.18 | 24.26 | 2.34 | 3.78 |
| $Fe_2O_3$ | % | 0.04 | 11.17 | 5.07 | 24.56 | 15.86 | 3.15 | 1.35 |
| MgO | % | 0.01 | 0.57 | 0.29 | 0.65 | 0.84 | 0.42 | 0.13 |
| CaO | % | 0.01 | 0.72 | 0.02 | 1.53 | 0.03 | 0.22 | 0.01 |
| $Na_2O$ | % | 0.01 | 0.07 | 0.03 | 0.08 | 0.05 | 0.04 | 0.02 |
| $K_2O$ | % | 0.01 | 1.77 | 2.25 | 2.81 | 6.2 | 0.50 | 0.94 |
| $TiO_2$ | % | 0.01 | 0.33 | 0.33 | 0.46 | 0.73 | 0.09 | 0.13 |
| $P_2O_5$ | % | 0.01 | 0.04 | 0.06 | 0.05 | 0.08 | 0.03 | 0.02 |
| MnO | % | 0.01 | 0.06 | <0.01 | 0.08 | <0.01 | 0.04 | <0.01 |
| $Cr_2O_3$ | % | 0.002 | 0.01 | 0.01 | 0.01 | 0.02 | 0.01 | 0.00 |
| TOT/C | % | 0.02 | 0.06 | 0.16 | 0.08 | 0.26 | 0.05 | 0.06 |
| TOT/S | % | 0.02 | 0.61 | 0.36 | 1.32 | 0.57 | 0.02 | 0.08 |
| Ba | mg kg$^{-1}$ | 1 | 511.75 | 1226.50 | 691 | 2474 | 326.00 | 433.00 |
| Cu | mg kg$^{-1}$ | 0.1 | 105.48 | 8.46 | 296.3 | 24.5 | 23.30 | 2.50 |
| Pb | mg kg$^{-1}$ | 0.1 | 10.33 | 154.28 | 22.1 | 774.8 | 3.80 | 15.90 |
| Zn | mg kg$^{-1}$ | 1 | 61.50 | 25.75 | 86 | 119 | 47.00 | 4.00 |
| Ni | mg kg$^{-1}$ | 0.1 | 36.25 | 3.68 | 89.8 | 8.4 | 13.60 | 1.50 |
| As | mg kg$^{-1}$ | 0.5 | 19.95 | 808.06 | 47.9 | 1641.7 | 4.40 | 319.40 |
| Sb | mg kg$^{-1}$ | 0.1 | 1746.15 | 4999.7 | 5660.00 | 11,560.00 | 203.30 | 757.60 |

**Table 3**
EPMA chemical composition (mean and standard deviation – stdeva in elemental %) of the main secondary Sb-bearing products identified in the slags and mill tailings.

| | Sb | | Fe | | As | | Ca | | S | | Total | | N |
|---|---|---|---|---|---|---|---|---|---|---|---|---|---|
| | Mean | Stdeva | Mean | Stdeva | Mean | Stdeva | Mean | Stdeva | Mean | Stdeva | Mean | Stdeva | |
| Tailings (%) | | | | | | | | | | | | | |
| $FeO_x$ | 6.8 | 3.8 | 39.9 | 6.7 | 1.1 | 3.8 | 0.2 | 0.1 | 0.5 | 0.4 | 69.2 | 5.8 | 26 |
| $FeSbO_x$ (tripuhyite) | 23.1 | 5.9 | 26.1 | 4.2 | 2.8 | 1 | 0.3 | 0.2 | 0.6 | 0.6 | 75.2 | 7.1 | 133 |
| Jarosite | 5.9 | 2.1 | 26.5 | 2.2 | 0.7 | 0.5 | 0.1 | 0.1 | 9.4 | 1.3 | 71 | 4.7 | 29 |
| Slags % | | | | | | | | | | | | | |
| $SbCaO_x$ (hydr-) oxycalciomeite | 42.7 | 8.4 | 2.1 | 0.8 | 0.3 | 0.3 | 7.2 | 0.8 | 0.3 | 0.1 | 75.3 | 7.1 | 5 |
| $FeO_x$ | 7.4 | 3.8 | 40.7 | 5.2 | 0.3 | 0.3 | 0.2 | 0.1 | 2.2 | 1.3 | 78.2 | 7.9 | 13 |
| $FeSbO_x$ (tripuhyite) | 26.2 | 8.7 | 24.3 | 6.1 | 0.6 | 0.5 | 0.8 | 1.5 | 2.4 | 1.9 | 85.5 | 9.5 | 36 |
| $SbO_x$ | 65 | 10 | 3.1 | 3.4 | 1.1 | 0.5 | 0.4 | 1.3 | 0.9 | 0.9 | 90.7 | 10.7 | 19 |

Micro-Raman spectra show differences according to the orientation of the minerals with sharp bands at 45, 87, 143, 161, 183, 196, 216, 307, 473 cm$^{-1}$ and a broader band centred at 707 cm$^{-1}$ (Fig. 4). Bands at 143, 186, and 307 cm$^{-1}$ are assigned to the contribution of stibnite (Frost et al., 2010). The other peaks are attributed to senarmontite, whose presence was confirmed by the μ-XRD patterns obtained on this well-crystalline phase (Fig. 5e). Large crystals of cristobalite and/or tridymite frequently contain 1 μm large inclusions of Sb-bearing phase, similar to valentinite (Fig. 5f). They may exhibit a rim of secondary products such as tripuhyite and show porosity filled with hematite and cervantite (Fig. 6b). Some grains of native antimony were also identified (Fig. 4). Among the iron (hydr-)oxides, goethite is the most enriched in Sb and contains Sb in variable amount. Fig. 8b shows goethite surrounded by a thin layer of pyrite and developed on a large troilite. This phase has a core with Sb ~9% when the outer part of the particle contain

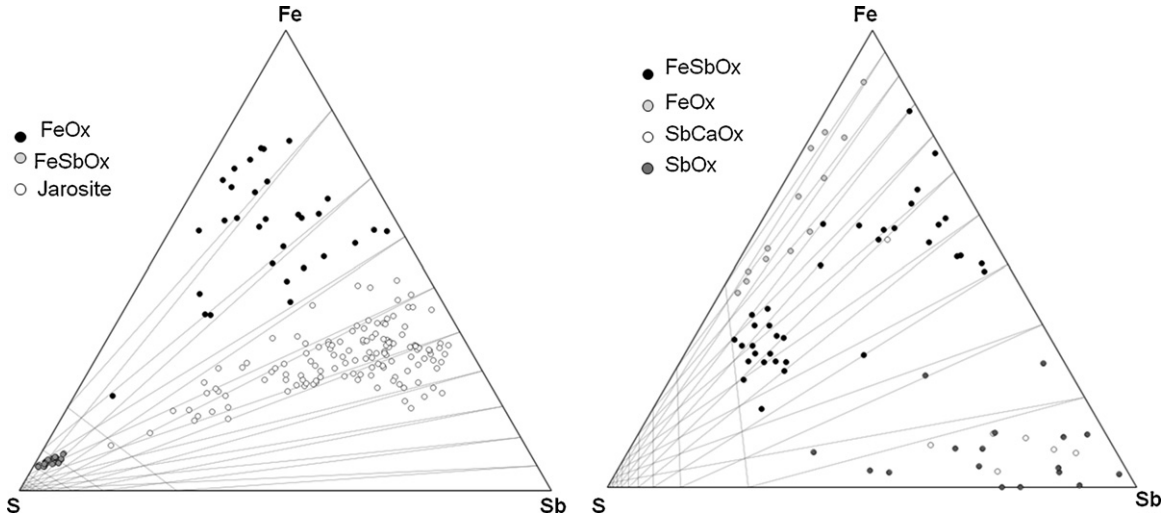


**Fig. 7.** Variability of the chemical composition of the main Sb-host phases in tailings and slags as shown in the ternary centered diagrams SFeSb according to EPMA data.

Please cite this article in press as: Courtin-Nomade, A., et al., Weathering of Sb-rich mining and smelting residues: Insight in solid speciation and soil bacteria toxicity. Chemie Erde - Geochemistry (2012), doi:10.1016/j.chemer.2012.02.004

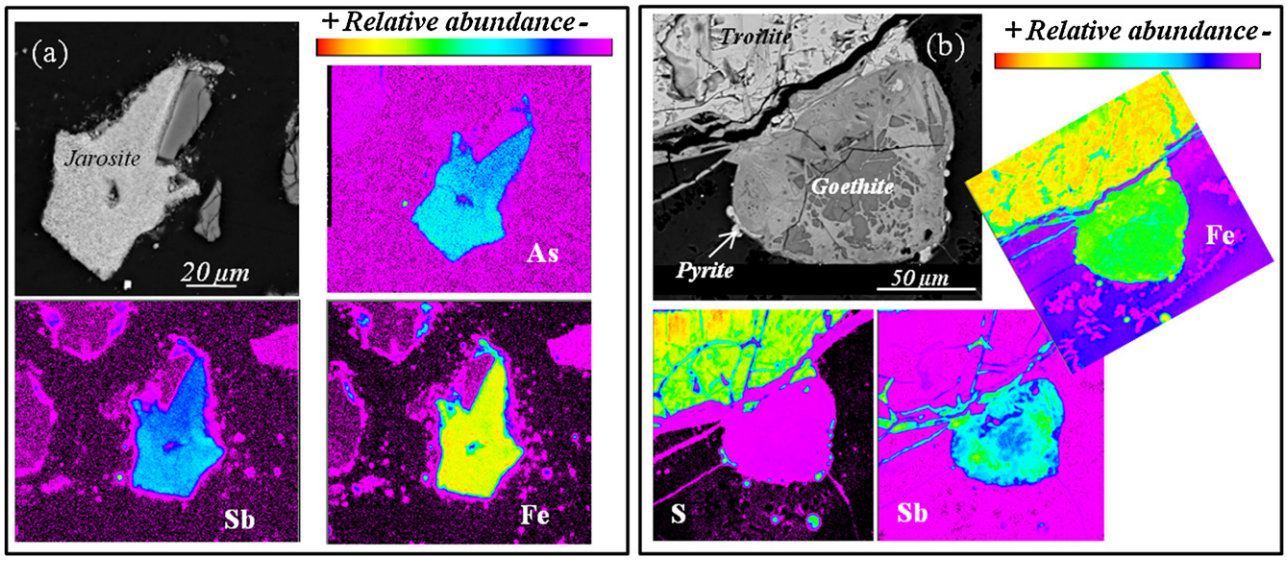


**Fig. 8.** EPMA elemental X-ray map of the metallic or metalloids host phases in (a) jarosite from tailings and (b) goethite associated to pyrite and troilite from slags.

11 < Sb% < 16. On the contrary to tailings material, Fe (hydr-)oxides barely contain As.

## 5. Discussion

### 5.1. Toxicity of antimony and arsenic

In this study, an experimental approach was used to investigate the effect of dissolved $As^{3+}$ and $Sb^{3+}$ onto microbial growth, as these two forms are present in the sulphides in the primary assemblages. As shown in Fig. 3, both metalloids severely affected biomass production. Growth inhibition varied between 0 and about 100% depending on bacterial strains and metalloid concentration, with Sb having inhibitory effects compared to As for a given concentration. In the case of antimony, the most sensitive isolates stop to proliferate at 10 and 50 mg $l^{-1}$ (*C. taiwanense* and *B. weihenstephanensis*, respectively), whereas in the case of arsenic, a clear growth inhibition was observed at 100–200 mg $l^{-1}$ (*C. taiwanense* and *Pseudomonas poae*). Among the tested bacteria, *Pseudomonas species* (NCS1, NCS3 and NCS4) seems to tolerate higher Sb and As concentrations compared to other species. In fact, *Pseudomonas species* are known to tolerate elevated concentration of several metals and metalloids such as Cr, Co, Ni, As, Cu, Cd (Achour et al., 2007; Appanna et al., 1996; Poirier et al., 2008). Several resistance/tolerance strategies toward metals and metalloids (contaminant binding onto the cell walls, proteins and extracellular polymers, metal precipitation or volatilization, active extrusion of contaminant from the cells) were developed by living organisms to survive in hostile conditions (Achour et al., 2007; Hughes and Poole, 1989; Shakya et al., 2011).

In the present study, different resistant/tolerant behaviour of bacteria relative to As and Sb were observed. For example, *B. weihenstephanensis*, the isolate characterized by a relatively high tolerance to As (more than 60% of growth at 200 mg $l^{-1}$), was quite sensitive to Sb (Fig. 3). This indicates that bacteria probably activated different resistance mechanisms to tolerate the presence of these two toxic ions. This is in agreement with the study of Achour et al. (2007) showing positive correlation between the antimonite sensitivity and the presence of the arsenic resistant genes.

Arsenite and antimonite can inhibit bacterial growth but at low concentration, they may also stimulate it. Positive effect of Sb was observed for *Pseudomonas poae* when subject to Sb concentrations of 10 mg $l^{-1}$ and for *Pseudomonas fluorescens* when exposed to 50 mg $l^{-1}$ of As. In fact, several heavy metals and metalloids are necessary for enzymatic functions and bacterial growth (Nithya et al., 2011), whereas at high concentration level, the same elements can block the essential functions in cells and thus exert an inhibitory action on microorganisms (Doelman et al., 1994).

We note that the negative effects of antimonite and arsenite, which were tested separately in our study, are probably underestimated because of possible toxicity enhancement upon a combined exposure of the cultured media to Sb and As. The formation of complexes with organic constituents or phosphates may cause a reduction of bioavailability and thus the toxicity of metalloids (Hughes and Poole, 1991).

### 5.2. Release of antimony in surface waters

Antimony concentrations measured in surface waters indicate a significant release, essentially from the former galleries (#2, Fig. 2). Antimony is, however, trapped in newly formed HFO precipitates at the main outlet (Sb = 0.27%). The highest concentration of Sb was observed near the former smelting site (#3, Fig. 2), which could be due to the leaching of the remaining slags or to unidentified groundwater inputs. No measurable impact of some potential discharge from the waste dump is reported after the heap (#4, Fig. 2). Similar observations have been reported by Wilson et al. (2004). Antimony concentrations range between 200 to 350 µg $l^{-1}$ from the outlet (pH = 6.2) or from the smelting site (pH ~ 7) independent of the pH value. Higher pH values downstream from the tailings dump are probably due to basic additives used during ore crushing processes before the flotation stage (e.g. $Na_2CO_3$ at pH = 8 added during the first crushing step; Périchaud, 1970). Indeed, no carbonate-rich geological formations were identified in the area and no acidification of the surface waters was observed despite the low pH of the tailings. Antimony concentration levels remain moderate compared to those reported in mine waters, for example by Ashley et al. (2003) (up to 55 mg $l^{-1}$ under near neutral conditions). Furthermore in the present study, detectable concentrations of Sb in surface waters were only measured in the area affected by mining activities. Indeed, reference samples (# 5 and 6, Fig. 2) corresponding to small tributaries of the "de Bussac" stream whose watersheds are located on areas not affected by anthropogenic activities, show very low concentrations (in November 2010, 2.4 < Sb < 2.7 µg $l^{-1}$).

Please cite this article in press as: Courtin-Nomade, A., et al., Weathering of Sb-rich mining and smelting residues: Insight in solid speciation and soil bacteria toxicity. Chemie Erde - Geochemistry (2012), doi:10.1016/j.chemer.2012.02.004

As a consequence, the presence of Sb in the geochemical background, if present at all, does not influence water concentrations of this element in the studied area. Similar levels were reported in surface waters as well as for other adits draining Sb veins and tailings in the same metallogenical district and other unaffected creeks in the district (Lansiart and Maubert, 1986). Furthermore, dilution effects and low discharge of the "de Bussac" stream would prevent the main river (the Alagnon river) to be affected by the former mining activities from Ouche.

The total amount of Sb can be estimated at around 2000 metric tons in the Ouche tailings. It constitutes a high potential hazard for the environment. Considering the permeability of the tailings estimated at around $10^{-5}$ m s$^{-1}$ according to their mean granulometry, future release depends on the flow rate percolating the waste residues (around 3500 m$^3$ year$^{-1}$ according to the mean annual rainfall), as well as on the degree of bioalteration processes and the reactivity of the solid Sb-bearing phases and natural attenuation. Studies dealing with the stability of Sb phases similar to those described in this study in secondary assemblages tend to indicate a low mobility of this element (Diemar et al., 2009; Filella et al., 2009) over a wide range of pH (3.7–8) (Flynn et al., 2003), in agreement with our observations.

### 5.3. Evolution of the primary assemblages in mill tailings and slags

Primary mineral assemblages found in flotation residues (i.e. mill tailings) and smelting slags show striking differences in the mineralogical assemblages which are mostly due to their very specific formation conditions.

Flotation residues include: (i) dominant gangue minerals such as quartz (from the ore veins and gneisses), feldspars, biotite (from gneisses) and muscovite, chlorite and phengite (from hydrothermally altered wall rocks) (Bril and Beaufort, 1989) and (ii) sulphides including remaining Sb sulphides (mainly stibnite and berthierite), which have not been extracted during ore treatment processes, as well as non-exploited sulphides such as pyrite and arsenopyrite, which were deposited by hydrothermal fluids along with the exploited minerals.

Smelting slags are generated by high-temperature metallurgical processes. As reported for numerous factories active during the 20th century (e.g., Ettler et al., 2001; Lottermoser, 2002), slags are mainly composed of various oxides (spinels), high temperature silicates (cristobalite and tridymite), and glass. Because of the alteration processes affecting the residues, several secondary products have been identified for which it is hard to decipher whether they are of hydrothermal (deuteric) or weathering origin. For instance, most of the clay minerals species found in mill tailings were already present as alteration products in the exploited ore (Bril and Beaufort, 1989). Except for iron, which is also present in biotite, sulphides were the main primary source of metals and metalloids. Waste materials studied here were submitted to leaching processes by meteoric and runoff waters since they were deposited (the mine was exploited since the 19th century and activities ended during the 1970s). As a result, several decades after the last deposition of residues, Ouche mill tailings barely contain minerals belonging to primary parageneses as very few primary sulphides (only pyrite) were detected in the heap. The relatively rapid kinetics of weathering was already noted by Ashley et al. (2003) under semiarid to humid climate. Combining dissolution experiments with field observations, they reported the influence of water/rock ratio variations. High water/rock ratios cause a direct dissolution of stibnite to $Sb^{5+}O_3$ accompanied by a high $H^+$ release. Low water/rock ratios induce the formation of Sb oxides (such as valentinite) with little acidification of waters. The large amount of metals/metalloids (e.g., Sb at >1%) still remaining in the studied tailings are secondary oxidized products or are associated with other authigenic phases. Indeed, Sb is mostly detected associated with sulphates or iron (hydr)oxides. The dominant sulphate containing Sb is jarosite that easily precipitates in the low pH conditions (~2.6) of the residues. High concentrations of up to 10% Sb have never been reported in jarosite. In fact, only minor integration of Sb in jarosite has been previously observed (Jamieson et al., 2005). We assume a substitution mechanism between $Sb^{5+}$ and $Fe^{3+}$ although this kind of substitution has only been described for dussertite $Ba(FeSb)_3(AsO_4)_2(OH, H_2O)_6$ which belongs to the alunite supergroup (crandellite group; Kolitsch et al., 1999).

Metals and metalloids can also be adsorbed on clay minerals or on amorphous iron compounds as described by Takahashi et al. (2010). In our study, clay minerals do not contain any detectable Sb and the only amorphous iron oxides are the precipitates observed at the outlet. However, Sb also participates in the formation of tripuhyite. Mitsunobu et al. (2011) noted that the formation of nanoparticulate tripuhyite precipitates by neutralization processes but very little data exist concerning the optimal conditions of formation of this mineral. On the studied site, acidic waste waters are mixed with neutral runoff waters but may also be neutralized by remaining chemical basic additives used during the ore processing, which may have triggered the precipitation of tripuhyite.

In the slag samples, minerals of primary parageneses can still be observed. However, the development of secondary minerals at the surface or along discontinuities of the slags indicates their reactivity in the on-site environmental context. On the contrary to tailing samples, sulphates are not observed in the smelting slags, which is expected due to the less acidic conditions. Many other Sb-bearing secondary phases found in slags are similar to those determined in tailings. These include iron (hydr-)oxides and tripuhyite. Some other products were only identified within slags samples like minerals belonging to the romeite group ($Ca_2Sb_2O_7$) with a composition close to the one of (hydr-)oxycalciоromeite (from $Ca_2Sb_2O_6O$ to $(Ca,Sb^{3+})_2(Sb^{5+},Ti)_2O_6(OH)$) (Atencio et al., 2010), as well as Sb oxides corresponding to senarmontite and valentinite. Romeite is known to be stable at high pH. Leaching of this mineral leads primarily to a loss of Ca rather than Sb (Cornelis et al., 2011). Senarmontite and valentinite are phases that are most likely to be formed under supergene conditions, however, hypogene formations have also been reported (Normand et al., 1996). All secondary products were found in vugs of smelting slags or coatings of the samples. Those hydroxides which are unambiguously formed under supergene conditions crystallize during smelting operations as evidenced by the textural relationships between Fe/Sb oxides with pyrite and troilite (Fig. 8b). However, from a quantitative point of view, the estimated potential release of metals or metalloids from slags is much lower than from tailings because of their relative proportion (~5% of the solid residues). The fact that sulphides are still present in the slags further suggest that this kind of residue is less sensitive to weathering and that slags are more stable under atmospheric conditions.

### 5.4. Comparing the behaviour of As and Sb

Because these elements are both metalloids and regarded as toxic substances (for Sb, see Filella et al., 2002; an abundant literature exists related to the toxicity of As e.g., see Mandal and Suzuki, 2002 for a review), the comparison of their fate in different environmental conditions is of a great interest (see Wilson et al., 2009 for a comparison of Sb and As behavior). The evolution of As-bearing minerals in mining environments was extensively studied on numerous examples (e.g. Courtin-Nomade et al., 2003; Filippi et al., 2004; Savage et al., 2000). Majzlan et al. (2007) studied tailings from a former mine with high As and Sb concentrations and noted that stibnite has completely disappeared, and is less stable

Please cite this article in press as: Courtin-Nomade, A., et al., Weathering of Sb-rich mining and smelting residues: Insight in solid speciation and soil bacteria toxicity. Chemie Erde - Geochemistry (2012), doi:10.1016/j.chemer.2012.02.004

than the associated berthierite. In our case, stibnite was identified in slag samples without any evidence for berthierite. This could be due to their abundance in the primary paragenesis, stibnite crystallizes after the berthierite formation and is more frequent than berthierite (Périchaud, 1970). Among the host phases identified at the Ouche site, jarosite appears to be as efficient for Sb immobilization as for As (see Savage et al., 2005 for As incorporation in jarosite). However, despite the fact that both of these metalloids are trapped by similar secondary phases, the processes of retention seem to be very different between them. For instance, large amounts of As may be incorporated in jarosite because of the substitution between $SO_4^{2-}$ and $AsO_4^{2-}$ whereas the incorporation of Sb into jarosite is likely by substitution between $Fe^{3+}$ and $Sb^{5+}$. Furthermore, Savage et al. (2005) highlighted that elevated As concentrations ($6.5 < As\ wt.\% < 43$) in synthetic jarosite affect their morphology. Jarosite with high As content is more anhedral and shows the presence of an amorphous phase associated with it. For the samples studied here, high Sb concentrations do not seem to involve any changes in the morphology of jarosite. Micro-XRD patterns obtained on Sb-rich jarosites (more than 10% of Sb) further indicate that they are still well-crystalline.

Majzlan et al. (2007) reported on the high capacity of iron containing minerals to retain Sb either by primary incorporation or secondary adsorption. This is confirmed in this study. No direct information concerning Sb speciation on iron (hydr-)oxides has been obtained but according to the Sb concentrations measured, e.g. in goethite, it may indicate the presence of $Sb^{3+}$, which is known to be more efficiently incorporated into goethite compared to $Sb^{5+}$. This is supported by the fact that Sb under its trivalent form is still present in both, the mill tailings and slag residues with (clino-) cervantite as the main $Sb^{3+}$ bearing phase. Furthermore, adsorption of Sb into Fe hydroxides is favoured in slags and tailings within the observed pH values (optimized range of sorption established between 2.5 and 7). Thus despite their similar chemical affinities, the association of Sb and As with potential host phases implies quite different chemical processes. There is thus no competition between these two metalloids for the same sorption site.

## 6. Conclusion

Arsenic and antimony inputs into natural environment can result in modifications of the composition or of the activity of the microbial communities. Negative effects (mortality or inhibition) were observed for all tested bacteria and for some of them even at very low concentration ($10\ mg\ l^{-1}$). In the Ouche tailings, Sb was found in very high concentrations (more than $10{,}000\ mg\ kg^{-1}$ in mine tailings) together with significant quantities of As. However, compared to the global contents and geological background, the release of Sb in solution remains low as indicated by their dissolved concentrations into the stream draining the former mine galleries and the heap. This indicates a global chemical stability of the residues. Although weathering was not favoured for water with neutral pH values, all primary Sb-bearing phases (stibnite and berthierite) originally disposed in the waste were almost completely replaced by large amounts of different secondary (oxidized) phases. This observation implies that Sb was redistributed *in situ* and that the great heterogeneity of authigenic phases results from very different local water/rock ratios. The various thermodynamic conditions prevailing in the heap paradoxically acts as a chemical barrier. Alteration processes seem to be more efficient in tailings than in slags even though slags are quantitatively a more important potential source for Sb.

## Acknowledgments

This study was financially supported by the Région Limousin during the thesis stage of O. Rakotoarisoa. We thank J. Cornette for access to the μRS facility in Limoges, C. Grosbois and N. Tamura for their support during ALS experiments and the ALS for beamtime access on the station 12.3.2. We are also very grateful to Patrice Fondanèche for the AAS analyses performed at the GRESE laboratory. The authors also thank the editor in chief, the associate editor, Pr. J. Majzlan, and the reviewers for their very useful comments that help to improve this manuscript. The Advanced Light Source is supported by the Director, Office of Science, Office of Basic Energy Sciences, U.S. Department of Energy under contract number DE-AC02-05CH11231.

## References

Achour, A.R., Bauda, P., Billard, P., 2007. Diversity of arsenite transporter genes from arsenic-resistant soil bacteria. Res. Microbiol. 158, 128–137.
Ackermann, S., Gieré, R., Newville, M., Majzlan, J., 2009. Antimony sinks in the weathering crust of bullets from Swiss shooting ranges. Sci. Total Environ. 407, 1669–1682.
Appanna, V.D., Gazs, L.G., St.Pierre, M., 1996. Multiple-metal tolerance in *Pseudomonas fluorescens* and its biotechnological significance. J. Biotechnol. 52, 75–80.
Ashley, P.M., Craw, D., Graham, B.P., Chappell, D.A., 2003. Environmental mobility of antimony around mesothermal stibnite deposits, New South Wales, Australia and Southern New Zealand. J. Geochem. Explor. 77, 1–14.
Ashley, P.M., Lottermoser, B.G., Collins, A.J., Grant, C.D., 2004. Environmental geochemistry of the derelict Webbs Consols mine, New South Wales, Australia. Environ. Geol. 46, 591–604.
Atencio, D., Andrade, M.B., Christy, A.G., Gieré, R., Kartashov, P.M., 2010. The pyrochlore supergroup of minerals: nomenclature. Can. Mineralogist 48, 673–698.
Bouchot, V., Ledru, P., Lerouge, C., Lescuyer, J.L., Milesi, J.P., 2005. Late Variscan mineralizing systems related to orogenic processes: The French Massif Central. Ore Geol. Rev. 27, 169–197.
Bril, H., Beaufort, D., 1989. Hydrothermal alteration and fluid circulation related to W, Au, and Sb vein mineralizations, Haut Allier, Massif Central, France. Econ. Geol. 84, 2237–2251.
Bril, H., Marignac, C., Tollon, F., Cuney, M., Boiron, M.C., 1994. Metallogenesis of the French Massif Central; time–space relationships between ore deposition and tectono-magmatic events. In: Keppie, J.D. (Ed.), Pre-Mesozoic Geology in France and Related Areas. Springer-Verlag, Berlin, pp. 379–402.
Casiot, C., Ujevic, M., Munoz, M., Seidel, J.L., Elbaz-Poulichet, F., 2007. Antimony and arsenic mobility in a creek draining an antimony mine abandoned 85 years ago (upper Orb basin, France). Appl. Geochem. 22, 788–798.
Cornelis, G., Gerven, T.V., Snellings, R., Verbinnen, B., Elsen, J., Vandecasteele, C., 2011. Stability of pyrochlores in alkaline matrices: solubility of calcium antimonite. Appl. Geochem. 26, 809–817.
Courtin-Nomade, A., Bril, H., Neel, C., Lenain, J.F., 2003. Arsenic in iron cements developed within tailings of a former metalliferous mine – Enguialès, Aveyron, France. Appl. Geochem. 18, 395–408.
Courtin-Nomade, A., Bril, H., Beny, J.M., Kunz, M., Tamura, N., 2010. Sulfide oxidation observed using micro-Raman spectroscopy and micro-X-ray diffraction – the importance of water/rock ratios and pH conditions. Am. Mineralogist 95, 582–591.
Craw, D., Wilson, N., Ashley, P.M., 2004. Geochemical controls on the environmental mobility of Sb and As at mesothermal antimony and gold deposits. Appl. Earth Sci. (Trans. Inst. Min. Metall. B) 113, B3–B10.
Diemar, G.A., Filella, M., Leverett, P., Williams, P.A., 2009. Dispersion of antimony from oxidizing ore deposits. Pure Appl. Chem. 81, 1547–1553.
Doelman, P., Jansen, E., Michels, M., Til, M., 1994. Effects of heavy metals in soil on microbial diversity and activity as shown by the sensitivity-resistance index, an ecologically relevant parameter. Biol. Fertil. Soils 17, 177–184.
Ettler, V., Legendre, O., Bodénan, F., Touray, J.C., 2001. Primary phases and natural weathering of old lead-zinc pyrometallurgical slag from Pribram, Czech republic. Can. Mineralogist 39, 873–888.
Filella, M., Belzile, N., Chen, Y.W., 2002. Antimony in the environment: a review focused on natural waters I. Occurrence. Earth Sci. Rev. 57, 125–176.
Filella, M., Philippo, S., Belzile, N., Chen, Y., Quentel, F., 2009. Natural attenuation processes applying to antimony: a study in the abandoned antimony mine in Goesdorf, Luxembourg. Sci. Total Environ. 407, 6205–6216.
Filippi, M., Goliáš, V., Pertold, Z., 2004. Arsenic in contaminated soils and anthropogenic deposits at the Mokrsko, Roudný, and Kašperské Hory gold deposits, Bohemian Massif (CZ). Environ. Geol. 45, 716–730.
Flynn, H.C., Meharg, A.A., Bowyer, P.K., Paton, G.I., 2003. Antimony bioavailability in mine soils. Environ. Pollut. 124, 93–100.
Frost, R.L., Bahfenne, S., Keeffe, E.C., 2010. Raman spectroscopic study of the mineral gerstleyite $Na_2(Sb, As)8S_{13}{\cdot}2H_2O$ and comparison with some heavy-metal sulfides. J. Raman Spectrosc. 41, 1779–1783.

Please cite this article in press as: Courtin-Nomade, A., et al., Weathering of Sb-rich mining and smelting residues: Insight in solid speciation and soil bacteria toxicity. Chemie Erde - Geochemistry (2012), doi:10.1016/j.chemer.2012.02.004

Grimalt, J.O., Ferrer, M., MacPherson, E., 1999. The mine tailing accident in Aznalcollar. Sci. Total Environ. 242, 3–11.
Jamieson, H.E., Robinson, C., Alpers, C.N., Nordstrom, D.K., Poustovetov, A., Lowers, H.A., 2005. The composition of coexisting jarosite-group minerals and water from the Richmond mine, Iron Mountain, California. Can. Mineralogist 43, 1225–1242, http://climat.meteofrance.com.
Hudson-Edwards, K.A., Macklin, M.G., Jamieson, H.E., Brewer, P.A., Coulthard, T.J., Howard, A.J., Turner, J.N., 2003. The impact of tailings dam spills and clean-up operations on sediment and water quality in river systems: The Ríños Agrio-Guadiamar, Aznalcoïllar, Spain. Appl. Geochem. 18, 221–239.
Hughes, M.N., Poole, R.K., 1989. Metals and Micro-organisms. Chapman and Hall, London.
Hughes, M.N., Poole, R.K., 1991. Metal speciation and microbial growth-the hard (and soft) facts. J. Gen. Microbiol. 137, 725–734.
Kolitsch, U., Slade, P.G., Tiekink, E.R.T., Pring, A., 1999. The structure of antimonian dussertite and the role of antimony in oxysalt minerals. Mineralogical Mag. 63, 17–26.
Kunz, M., Tamura, N., Kai Chen, K., MacDowell, A.A., Celestre, R.S., Church, M.M., Fakra, S., Domning, E.E., Glossinger, J.M., Kirschman, J.L., Morrison, G.Y., Plate, D.W., Smith, B.V., Warwick, T., Yashchuk, V.V., Padmore, H.A., Ustundag, E., 2009. A dedicated superbend X-ray microdiffraction beamline for materials, geo-, and environmental sciences at the advanced light source. Rev. Sci. Instrum. 80, art. no 035108.
Ledru, P., Lardeaux, J.-M., Santallier, D., Autran, A., Quenardel, J.-M., Lerouge, G., Floc'h, J.-P., Maillet, N., Marchand, J., Ploquin, A., 1989. Où sont les nappes du Massif Central Français? Bulletin de la Société Géologique de France 3, 605–618.
Lansiart, M., Maubert, F., 1986. Impacts cumulés d'anciennes mines sur le bassin versant hydrologique du Céroux (Cantal, Haute-Loire). Unpub. rapport BRGM 86 SGN 724 GEG, 105 p.
Lottermoser, B.G., 2002. Mobilization of heavy metals from historical smelting slag dumps, north Queensland, Australia. Mineralogical Mag. 66, 475–490.
Macklin, M.G., Brewer, P.A., Balteanu, D., Coulthard, T.J., Driga, B., Howard, A.J., Zaharia, S., 2003. The long term fate and environmental significance of contaminant metals released by the January and March 2000 mining tailings dam failures in Maramureş County, upper Tisa Basin, Romania. Appl. Geochem. 18, 241–257.
Majzlan, J., Lalinská, B., Chovan, M., Jurkovič, L., Milovská, S., Göttlicher, J., 2007. The formation, structure, and ageing of As-rich hydrous ferric oxide at the abandoned Sb deposit Pezinok (Slovakia). Geochim. Cosmochim. Acta 71, 4206–4220.
Majzlan, J., Lalinská, B., Chovan, M., Bläß, U., Brecht, B., Göttlicher, J., Steininger, R., Hug, K., Ziegler, S., Gescher, J., 2011. A mineralogical, geochemical, and microbiogical assessment of the antimony- and arsenic-rich neutral mine drainage tailings near Pezinok, Slovakia. Am. Mineral. 96, 1–13.
Mandal, B.K., Suzuki, K.T., 2002. Arsenic round the world: a review. Talanta 58, 201–235.
Mitsunobu, S., Takahashi, Y., Utsunomiya, S., Marcus, M.A., Terada, Y., Iwamura, T., Sakata, M., 2011. Identification and characterization of nanosized tripuhyite in soil near Sb mine tailings. Am. Mineral. 96, 1171–1181.
Murata, T., Kanao-Koshikawa, M., Takamatsu, T., 2005. Effects of Pb, Cu, Sb, In and Ag contamination on the proliferation of soil bacterial colonies, soil dehydrogenase activity, and phospholipid fatty acid profiles of soil microbial communities. Water Air Soil Pollut. 164, 103–118.
Nithya, C., Gnanalakshmi, B., Pandian, S.K., 2011. Assessment and characterization of heavy metal resistance in Palk Bay sediment bacteria. Mar. Environ. Res. 71, 283–294.
Normand, C., Gauthier, M., Jébrak, M., 1996. The Quebec antimony deposit: an example of Gudmundite-Native Antimony. Mineralization the Ophiolitic Mélange of the Southeastern Québec Appalachians. Econ. Geol. 91, 149–163.
Périchaud, J.J., 1970, Les gisements métalliques du district à antimoine de Brioude-Massiac (Massif Central français). Unpub. thèse d'Etat, Université de Clermont-Ferrand II, 5 v., 771 p.
Poirier, I., Jean, N., Guary, J.C., Bertrand, M., 2008. Responses of the marine bacterium *Pseudomonas fluorescens* to an excess of heavy metals: physiological and biochemical aspects. Sci. Total Environ. 406, 76–87.
Savage, K.S., Tingle, T.N., O'Day, P.A., Waychunas, G.A., Bird, D.K., 2000. Arsenic speciation in pyrite and secondary weathering phases, Mother Lode Gold District, Tuolumne County, California. Appl. Geochem. 15, 1219–1244.
Savage, K.S., Bird, D.K., O'Day, P.A., 2005. Arsenic speciation in synthetic jarosite. Chem. Geol. 215, 473–498.
Scheinost, A.C., Rossberg, A., Vantelon, D., Xifra, I., Kretzschmar, R., Leuz, A.-K., Funke, H., Johnson, C.A., 2006. Quantitative antimony speciation in shooting-range soils by EXAFS spectroscopy. Geochim. Cosmochim. Acta 70, 3299–3312.
Shakya, S., Pradhan, B., Smith, L., Shrestha, J., Tuladhar, S., 2011. Isolation and characterization of aerobic culturable arsenic-resistant bacteria from surfacewater and groundwater of Rautahat District, Nepal. J. Environ. Manage., 1–6.
Takahashi, T., Shozugawa, K., Matsuo, M., 2010. Contribution of amorphous iron compounds to adsorptions of pentavalent antimony by soils. Water Air Soil Pollut. 208, 165–172.
Takaoka, M., Kukutani, S., Yamamoto, T., Horiuchi, M., Satta, N., Takeda, N., Oshita, K., Yoneda, M., Morisawa, S., Tanaka, T., 2005. Determination of chemical form of antimony in contaminated soil around a smelter using X-ray absorption fine structure. Anal. Sci. 21, 769–773.
Tamura, N., Padmore, H.A., Patel, J.R., 2005. High spatial resolution stress measurements using synchrotron based scanning X-ray microdiffraction with white or monochromatic beam. Mater. Sci. Eng., A 399, 92–98.
Therese, K.L., Bartell, J., Deepa, P., Mangaiyarkarasi, S., Ward, D., Dajcs, J., Madhavan, H.N., Stroman, D., 2009. DNA sequencing by Microseq kit targeting 16S rRNA gene for species level identification of mycobacteria. Indian J. Med. Res. 129, 176–181.
Wang, Q., He, M., Wang, Y., 2011. Influence of combined pollution of antimony and arsenic on culturable soil microbial populations and enzyme activities. Ecotoxicology 20, 9–19.
Wilson, N.J., Craw, D., Hunter, K., 2004. Contributions of discharges from a historic antimony mine to metalloid content of river waters, Marlborough, New Zealand. J. Geochem. Explor. 84, 127–139.
Wilson, S.C., Lockwood, P.V., Ashley, P.M., Tighe, M., 2009. The chemistry and behaviour of antimony in the soil environment with comparisons to arsenic: a critical review. Environ. Pollut. 158, 1169–1181.
WHO (World Health Organization), 2008. Guidelines for Drinking-water Quality. 3rd edition incorporating the 1st and 2nd addenda. Vol. 1, Recommendations, 668 p.

Please cite this article in press as: Courtin-Nomade, A., et al., Weathering of Sb-rich mining and smelting residues: Insight in solid speciation and soil bacteria toxicity. Chemie Erde - Geochemistry (2012), doi:10.1016/j.chemer.2012.02.004